JOURNAL OF GEOPHYSICAL RESEARCH, VOL. 98, NO. C4, PAGES 6991–6999, APRIL 15, 1993

Deep Currents and the Eastward Salinity Tongue in the Equatorial Atlantic: Results From an Eddy-Resolving, Primitive Equation Model

CLAUS W. BÖNING AND FRIEDRICH A. SCHOTT

Institut für Meereskunde an der Universität Kiel, Kiel, Germany

The high-resolution model of the wind-driven and thermohaline circulation in the Atlantic Ocean developed in recent years as a "community modeling effort" for the World Ocean Circulation Experiment is examined for the temporal and spatial structure of the deep equatorial current field and its effect on the spreading of North Atlantic Deep Water (NADW). Under seasonally varying wind forcing, the model reveals a system of basin-wide zonal currents of $O(5$ cm s$^{-1})$, alternating east-west, and oscillating at an annual period. The current fluctuations are induced by the seasonal cycle of the wind stress in the equatorial Atlantic and show characteristics of long equatorial Rossby waves with westward phase propagation of about 15 cm s^{-1}. The mean flow in the deep western tropical Atlantic is governed by a deep western boundary current (DWBC) with core velocities of more than 10 cm s^{-1}. Only a small fraction of the DWBC branches off at the equator, with correspondingly low mean eastward currents of only about 1 cm s^{-1}. Despite this weak advection along the equator, a well-developed salinity tongue is observed in the model, which is reminiscent of observed property distributions at the upper NADW level. The model evaluation indicates the salinity pattern to be a result of a balance between mean zonal advection and meridional diffusion of salt. The presence of the zonal current oscillations appears to have no significance for the existence of the salinity tongue.

1. INTRODUCTION

It is an important property of present climate conditions that the meridional transport of heat in the Atlantic Ocean is not symmetrical with respect to the equator but northward everywhere. The asymmetry is caused by the structure of the thermohaline circulation: The southward spreading of cold and saline North Atlantic Deep Water (NADW), formed in the Labrador Sea and north of Iceland, is compensated by a northward, cross-equatorial flux of warmer surface water. The bulk of NADW is carried by the deep western boundary current (DWBC) which has been identified as a continuous signal along the continental slope in the subtropical North Atlantic [*Fine and Molinari*, 1988]. An important, yet unsettled issue concerns the behavior of the DWBC near the equator. The distribution of water mass properties like salinity, oxygen, and nutrients [*Wüst*, 1935; *Kawase and Sarmiento*, 1986] or anthropogenic tracers like chlorofluorocarbons [*Weiss et al.*, 1985] suggests that only part of the upper NADW crosses the equator near the American continental slope and that a significant fraction appears in a wedge extending eastward along the equator (Figure 1). Lacking sufficient data to estimate the mean current field, one is tempted to conclude a branching of the DWBC in the equatorial Atlantic. However, the linear model study of *Kawase* [1987] indicated that an equatorially confined steady flow could appear only in an ocean with strong damping of long Rossby waves. In the asymptotic state of a recent numerical spin-up experiment by *Kawase et al.* [1992], nearly all the mass transport in the DWBC crossed the equator, a behavior similar to that seen in large-scale circulation models, e.g., in the NADW depth range of the global eddy-resolving model of *Semtner and Chervin* [1992]. The model results presented here will show that an eastward flow along the equator of only $O(1$ cm s$^{-1})$ may not be incompatible with the observed tracer distribution.

There is only little information about the deep current structure in the equatorial Atlantic. Direct current measurements have been reported from a single station at 30°W. *Ponte et al.* [1990] show a vertical profile of velocity down to 4000 m indicating predominantly zonal currents of 10–20 cm s^{-1} amplitude, alternating in the east-west direction with depth. The same station, originally occupied in January 1989, was revisited during *Meteor* cruise M16/3 in June 1991. Figure 2*a* shows the upper 2000 m of the zonal velocity profiles. While the vertical structure appears fairly similar in both profiles, the currents are in opposite direction nearly everywhere below 700-m depth. There is some similarity of the current patterns with the "stacked jets" observed in the equatorial Pacific and Indian oceans. In these oceans there is accumulating evidence that zonal jets with long time scales and short vertical scales represent a dominant feature of the deep equatorial circulation [*Luyten and Swallow*, 1976; *Eriksen*, 1981; *Firing*, 1987; *Ponte and Luyten*, 1989, 1990]. However, as was noted by *Ponte et al.* [1990], both the vertical scale and the amplitude of the currents measured at 30°W appear larger than those of the stacked jets in the Pacific and Indian Oceans.

The only existing longer-period current record at the upper NADW level from the equatorial interior of the Atlantic was reported by *Weisberg and Horigan* [1981], who found, at 3°W and 1822-m depth, persistent eastward currents of 15–30 cm s^{-1} during the time period July–November 1977 (Figure 2*b*). However, as recent measurements with SOFAR floats at the 1800-m level suggest [*Richardson and Schmitz*, 1993], this seemingly persistent eastward flow might only be part of a longer-period variability of the deep equatorial current system. Ensemble-averaged velocities from the SOFAR floats between 2.5°S and 2.5°N, and between 20°W and 40°W, were eastward (~4.1 cm s^{-1}) from February 1989 to February 1990 and westward (~4.6 cm s^{-1}) from March 1990 to November 1990, though it has to be

Paper number 92JC02815.
0148-0227/93/92JC-02815$05.00

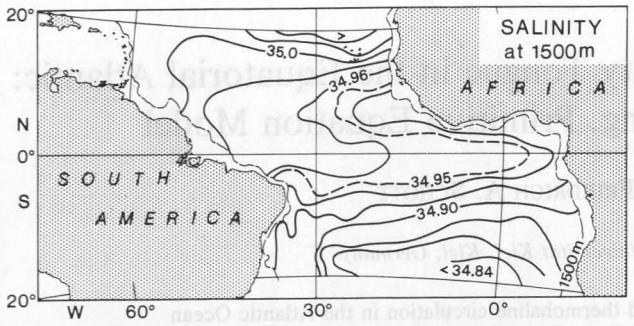

Fig. 1. Distribution of salinity (in practical salinity units) at 1500-m depth in the tropical Atlantic (courtesy of J. Reid, unpublished work).

noted that it could not be monitored whether the floats stayed at the same depth throughout the entire observational period. In the water mass properties, the depth range of 1500–1700 m along the equator, i.e., the depth range of upper NADW, is characterized by a core of high chlorofluorocarbon (CFC) concentration, extending eastward from the western boundary [*Weiss et al.*, 1985]. The mean advection rates inferred from the property distributions are $O(1$ cm $s^{-1})$ (M. Rhein, personal communication, 1992). This is much smaller than the current amplitudes shown in instantaneous velocity profiles or existing moored records, obviously rendering reliable estimates of the mean flow from direct current observations very difficult.

In the present study we shall examine the temporal and spatial structure of the deep velocity field and the relative roles of mean advection and fluctuations in the eastward spreading of NADW properties using a high-resolution model of the wind-driven and thermohaline circulation in the Atlantic Ocean. The model was developed in recent years [*Bryan and Holland*, 1989] as a "community modeling effort" (CME) for the World Ocean Circulation Experiment (WOCE). Following the initial experiment described by *Bryan and Holland* [1989], a number of runs differing in resolution, friction, and wind forcing have been performed [e.g., *Böning et al.*, 1991]. Evaluations of the upper layer circulation in the western equatorial Atlantic indicated a fairly successful simulation of the general features of the observed seasonal circulation changes [*Schott and Böning*, 1991; *Didden and Schott*, 1992]. A notable difference of the CME results compared to previous studies was a concentration of the zonal currents in high-velocity bands, resulting, e.g., in two separate cores in the North Equatorial Countercurrent (NECC) region. The model examination shall be extended here to the deeper layers.

2. Model Experiments

The model of the wind-driven and thermohaline circulation in the Atlantic Ocean between 15°S and 65°N was developed by *Bryan and Holland* [1989] on the basis of the primitive equation model described by *Bryan* [1969] and *Cox* [1984]. The thermohaline circulation is driven by a relaxation of surface salinity to the monthly mean values of *Levitus* [1982] and a heat flux according to the linear formulation of *Han* [1984]. The initial experiment performed at the U.S. National Center for Atmospheric Research (NCAR) was a 25-year simulation starting from the temperature and salinity fields of *Levitus* [1982]. Based on the first 20 years of this spin-up is a sequence of experiments at both NCAR and the Institut für Meereskunde, Universität Kiel (IfM Kiel), exploring the model sensitivity to resolution, friction and wind forcing. We shall focus here on three experiments performed at IfM Kiel.

Case A is an experiment with high horizontal resolution ($\frac{1}{3}$° latitudinal, and 0.4° longitudinal grid spacing), forced with the monthly mean wind stresses of *Hellerman and Rosenstein* [1983]. Constant coefficients (-2.5×10^{19} cm^4 s^{-1}) for the biharmonic lateral friction and diffusivity were used. The analysis is based on the 5-year period between model years 20.0 and 25.0.

Case B is a sensitivity experiment forced with a steady wind stress, i.e., the January conditions of *Hellerman and Rosenstein* [1983]. Resolution and friction are the same as in the standard case A. This case was initialized at year 25.0 of A and integrated for 4 years. A variant of this experiment (case B1) was performed with steady wind stress only in the equatorial Atlantic, south of 10°N. In a transition zone between 10° and 15°N the January winds were linearly merged with the seasonal winds to the north.

Case C is a sensitivity experiment with coarse resolution (1° × 1.2° grid spacing) and the same forcing as in case A. A Laplacian formulation for the lateral friction was used here

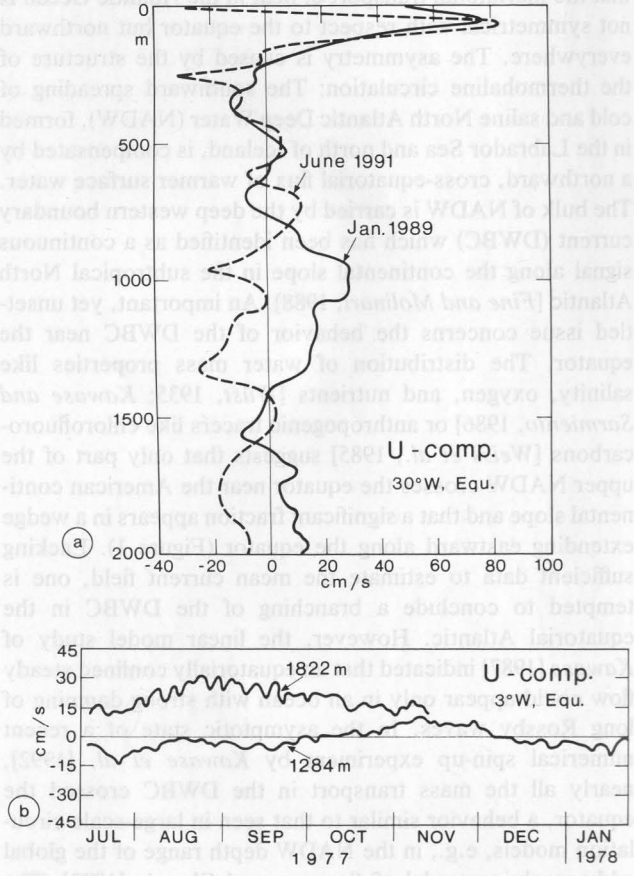

Fig. 2. (*a*) Zonal velocity as a function of depth, in the equatorial Atlantic at 0°N, 30°W, observed in January 1989 [*Ponte et al.*, 1990] and during *Meteor* cruise M16/3 in June 1991. (*b*) Low-pass-filtered time series of east component of currents at 3°W, 1284-m and 1822-m depth, during July 1977 to January 1978 [from *Weisberg and Horigan*, 1981].

with eddy coefficients decreasing in the vertical from 2×10^7 $cm^2\ s^{-1}$ at the top to 0.5×10^7 $cm^2\ s^{-1}$ below 2000 m.

The vertical grid configuration is the same in all cases: 30 vertical grid boxes are used; the grid spacing increases smoothly from 35 m at the surface to 100 m near 500-m depth and 250 m at 1000-m depth; from there on, vertical resolution stays constant. All experiments also used the same eddy coefficients for vertical viscosity (10 $cm^2\ s^{-1}$) and diffusivity (0.3 $cm^2\ s^{-1}$).

3. Deep Current Field and Salinity Distribution

Maps of salinity at a level (1875 m) corresponding to the upper NADW are shown in Figure 3. In the initial conditions, given by the smoothed climatological data set of *Levitus* [1982], there is an indication of more saline water along the equator, but gradients are generally weak (Figure 3*a*). The mean salinity pattern of the high-resolution case A, averaged over a 5-year period, is shown in Figure 3*b*. The most saline water spreads southward along the South American continental slope. The tongue of saline water extending eastward in the equatorial Atlantic is more prominent than in the initial conditions. At first impression the salinity pattern bears similarities to the observed distribution of NADW

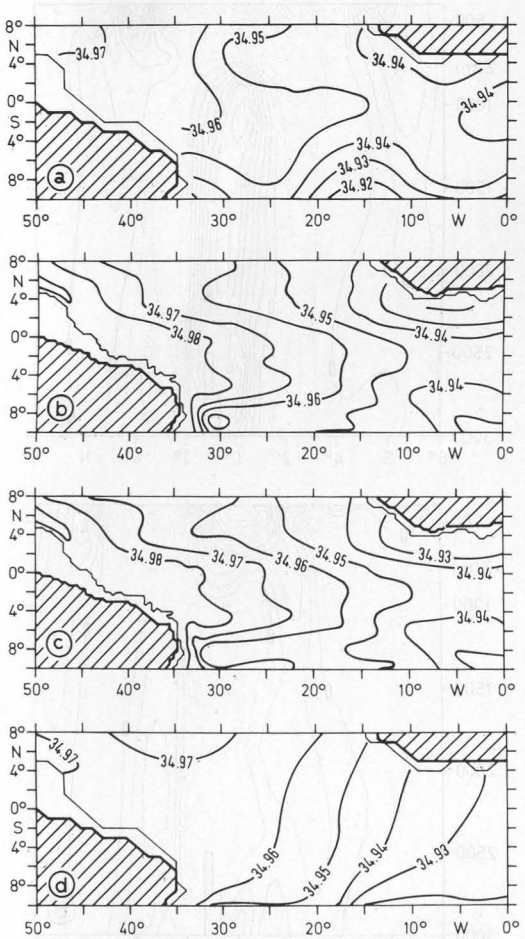

Fig. 3. Maps of mean salinity in the tropical Atlantic at 1875-m depth (contour interval 0.01) (*a*) the initial conditions of the model given by the climatology of *Levitus* [1982]; (*b*) a 5-year average of the high-resolution case A; (*c*) the same quantity averaged over the last year of case B; (*d*) the solution of the coarse-resolution case C after 25 years of integration.

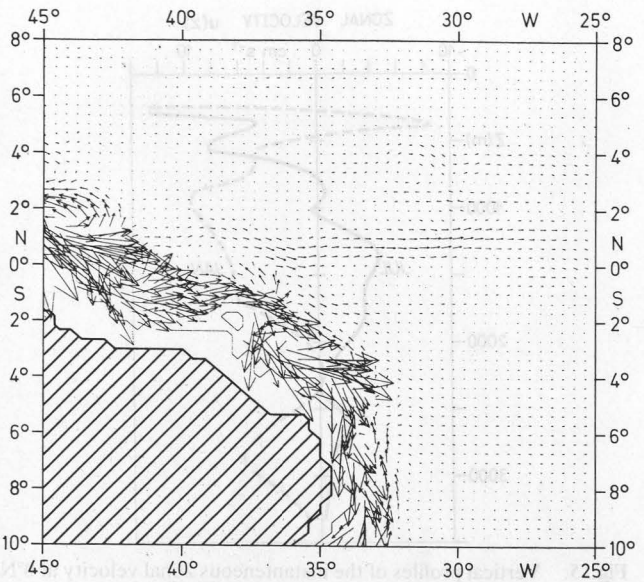

Fig. 4. Mean velocity field at 1875-m depth for the high-resolution model (case A).

properties in the tropical Atlantic. There is a notable difference, however. The salinity tongue in the model is not symmetrical about the equator and appears broader than observed. At 30°W, highest salinities are found not at 0°, but at 4°S. Model case B, with constant wind forcing, gives essentially the same result (Figure 3*c*). However, the integration with the coarse-resolution model (case C) leads to a very different distribution (Figure 3*d*). The eastward salinity wedge along the equator is erased; instead, salinity smoothly decreases from west to east, indicating a much stronger role of diffusion relative to zonal advection than in the high-resolution case.

Figure 4 shows a map of the 5-year mean velocity field of the model (case A), for the western tropical Atlantic at the upper NADW level. The DWBC appears as a continuous signal along the continental slope; core speeds are 10–20 cm s^{-1}. The bulk of the flow seems to penetrate into the southern hemisphere without significant branching at the equator. However, there is a mean eastward flow along the equator, though weak. The maximum eastward velocities found in the high resolution cases A and B are $O(1\ cm\ s^{-1})$. There is only a very weak eastward flow ($<0.2\ cm\ s^{-1}$) in the solution of the coarse-resolution case C. Before exploring the mean flow pattern in some more detail, we will first examine the temporal variability of the equatorial flow regime.

Figure 5 shows two instantaneous vertical profiles of u at 0°N, 30°W for case A. The strong Equatorial Undercurrent (EUC) is not shown in this representation. (For an account of the upper layer circulation, the reader is referred to *Schott and Böning* [1991].) The magnitude of the zonal velocities in January and July is much higher than the mean annual velocities. The temporal reversal of the zonal flow pattern appears somewhat similar to the observed instantaneous profiles displayed in Figure 2*a*. However, the model lacks the smaller vertical scales of the observations.

The spatial structure of the time-dependent zonal flow of case A is illustrated in Figure 6, showing meridional sections of mean zonal velocity along 30°W for two seasons, spring

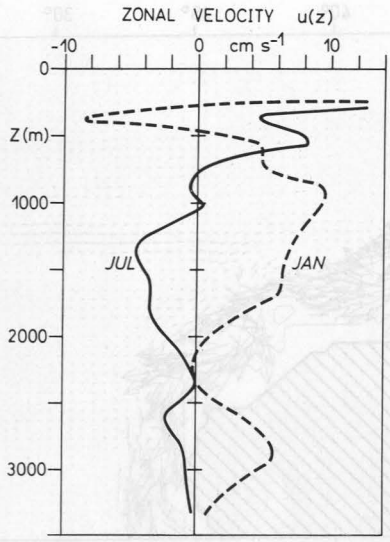

Fig. 5. Vertical profiles of the instanteneous zonal velocity at 0°N, 30°W, in January and July; model case A.

and fall. As has been demonstrated by *Schott and Böning* [1991], the model reproduces the general features of the observed seasonal current changes in the upper layers, except for probably too pronounced jet cores. For the deep currents a comparison is difficult, since not much is known about the current structure in the deeper layers of the interior equatorial Atlantic beyond the vertical profiles and current time series shown in Figure 2. The model yields a system of deep zonal currents alternating in direction eastward and westward with latitude. These current bands extend nearly over the entire width of the basin. Their velocity is strongest (>5 cm s^{-1} in the seasonal averages) near the equator and decreases to about 1 cm s^{-1} at 6° latitude. The deep current signal is also present but much weaker in the coarse-resolution model (case C), with maximum zonal velocities at the equator of only about 0.5 cm s^{-1}. Between the two seasons shown in Figure 6 there is a reversal of the current direction in nearly all parts of the section.

The temporal variation of the high-resolution case A is illustrated further in Figure 7, showing a longitude-time plot of zonal velocity at 1875-m depth along the equator, over a period of 2 model years. Apart from some higher-frequency variability, there is a clear signature of a large-scale wave pattern with a period of 1 year, and a westward phase velocity of about 15 cm s^{-1}, indicative of long equatorial Rossby waves. To examine the role of the annual cycle of wind stress in generating the deep current oscillations, the model was integrated for 4 more years over which the wind stress was kept constant at its January state (case B). The resulting phase diagram of the first 2 years is shown in Figure 8. While the wave pattern remains visible during the first 1 or 1.5 years, its amplitude is continuously decreasing. After 1.5 years the westward propagating signal has faded away. In an additional experiment (case B1), the first 2 years of case B were repeated with the wind stress held constant only in the equatorial region south of 10°N. The result was a very similar spin-down as shown in Figure 8. The zonal current bands of case A have to be regarded therefore as a deep baroclinic response to the seasonal variation of wind forcing in the equatorial Atlantic.

In contrast to the zonal velocity field, which is dominated by the deep seasonal response, the meridional velocity component v in both high-resolution cases A and B is subject to fluctuations of higher frequency. Figure 9 shows longitude-time plots of v at 1875-m depth along the equator. Waves of roughly 1000-km wavelength and period of 1.5 months appear as a prominant signal over nearly the whole zonal extent of the basin. The Hovmoeller diagrams clearly reveal a westward phase, and eastward group velocity, characteristical of Rossby-gravity (Yanai) waves. Similar deep oscillations, but with a predominant period of 30 days, were obtained in other multilevel models [e.g., *Cox*, 1980; *Philander et al.*, 1986]. The signature of such waves can be seen in the deep current measurements by *Weisberg and Horigan* [1981] in the central equatorial Atlantic. According to the analysis of *Cox* [1980], the Rossby-gravity waves in the deeper layers are excited by instabilities of the strong zonal currents near the surface, from where energy is radiated downward and eastward along ray paths predicted from linear theory. Thus the wave period should be mainly controlled by the instability properties of the upper layer

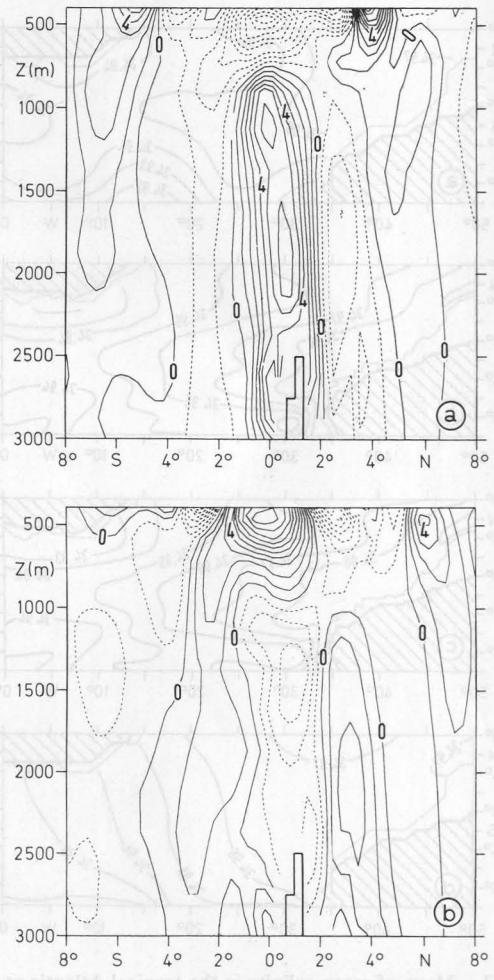

Fig. 6. Meridional sections of zonal velocity at 30°W, model case A: 5-year averages for (*a*) spring season, April-May-June, and (*b*) fall season, October-November-December. Contour interval is 1 cm s^{-1}. Negative values (dashed contours) correspond to westward flow.

flow, i.e., the period of the most unstable wave. Factors affecting the nature of the instabilities in the equatorial regime have been studied by *McCreary and Yu* [1992] with an idealized $2\frac{1}{2}$-layer model; they noted a rich spectrum of disturbances between 15 and 50 days.

There are some interesting differences between the surface and deeper layer oscillations in the present model. In model case A the meridional velocity fluctuations at the surface are strongly modulated with season. Maximum amplitudes (>40 cm s^{-1}) occur during fall (when the NECC is strong), between 15° and 35°W. At this time, shorter periods (<30 days) seem to prevail. The near-surface oscillations are different in case B where there is no seasonality and no NECC. In that case, waves with weaker amplitudes (about 15 cm s^{-1}) and periods of 30–40 days occur mainly between 20° and 30°W. In contrast to the surface layer, both model cases show rather similar wave patterns in the deep layer, with an energy maximum at periods of about 45 days (Figure 9). This suggests that the presence of the NECC and shear instabilities of the NECC–South Equatorial Current system do not play a leading role in generating the deep Rossby-gravity waves as seen in Figure 9. The connection between the upper layer instability and the wave field in the deeper layers, and the cause of the rather long period of the deep Yanai waves in the present model needs further investigation.

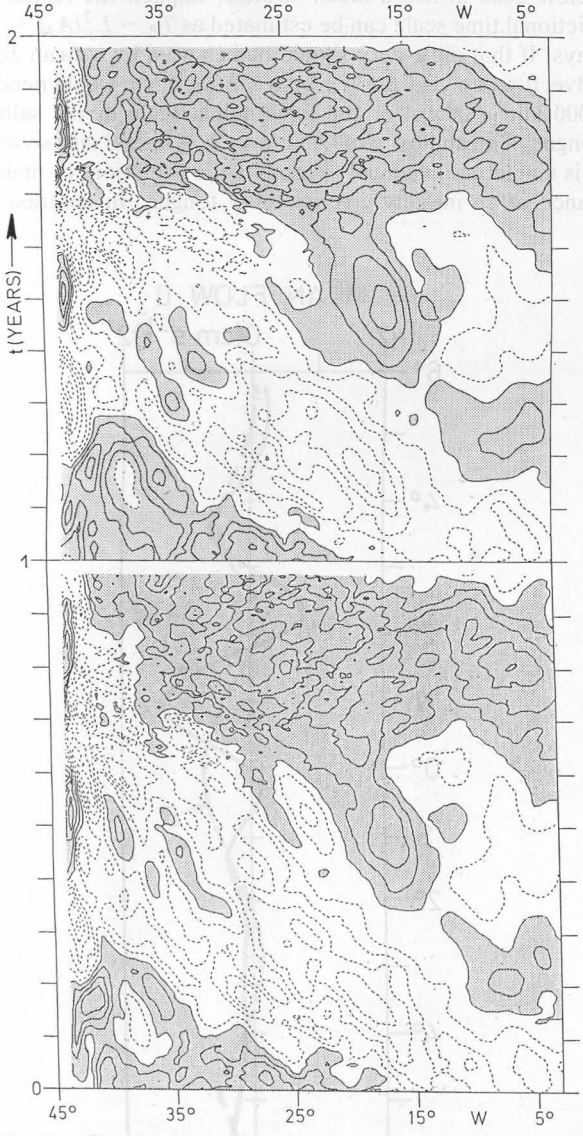

Fig. 7. Time-longitude diagram of the zonal current component at 1875-m depth, along the equator; contour interval is 2 cm s^{-1}. The stippled areas correspond to eastward flow. Model case A.

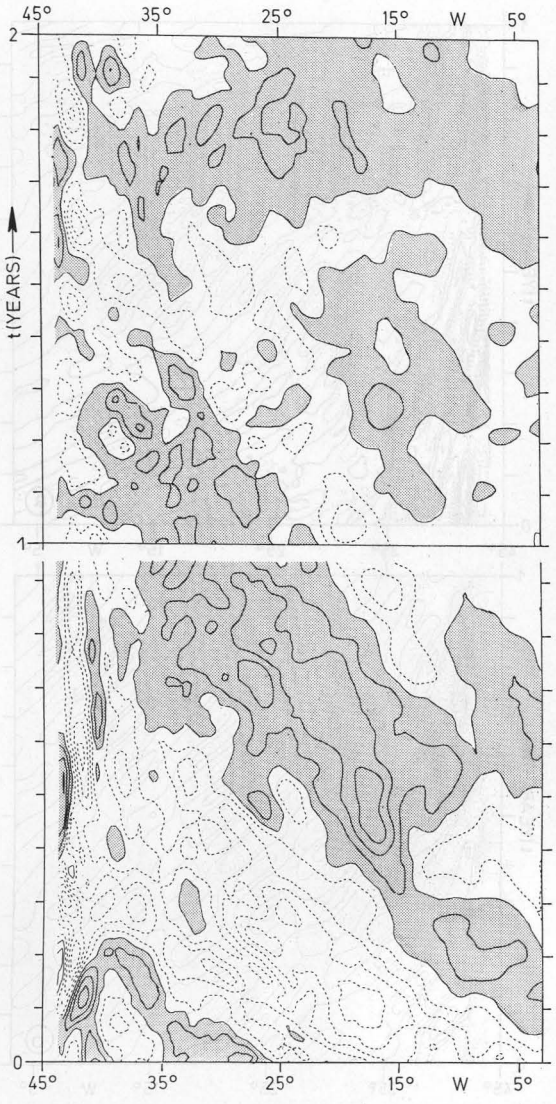

Fig. 8. The same as in Figure 7, except for case B (first 2 years) in which the wind stress was held constant at its January state.

4. Role of Mean Flow and Oscillations for the Eastward Salinity Wedge: A Scale Analysis

Although the zonal current bands of annual period are much more energetic than the mean zonal flow, their net effect on the mean salinity distribution appears to be negligible: Figure 3*c* shows that after four years of integration without seasonal forcing there is almost no difference to the salinity pattern of the seasonally forced model (Fig. 3*b*). The model results therefore suggest that the advection by the mean flow should play the leading role in the salinity budget. Meridional profiles of the mean flow at 30°W, for model cases A and B, are shown in Figure 10. Maximum eastward

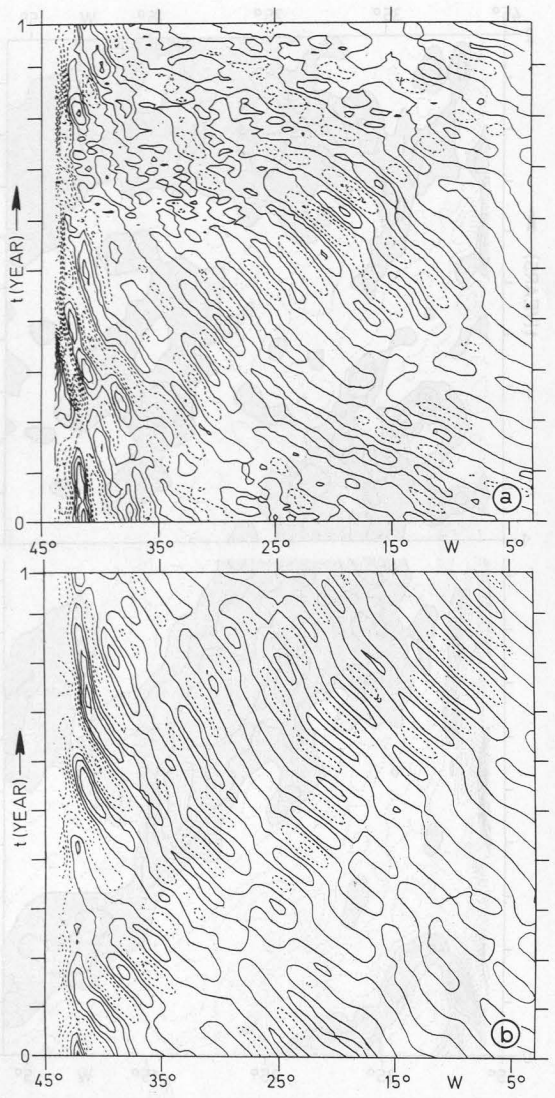

Fig. 9. Longitude-time plot of the meridional velocity component v at 1875-m depth, along the equator, for 1 year of (a) model case A and (b) case B. Contour interval is 2 cm s^{-1}.

velocities near the equator are about 1 cm s^{-1}. The pattern in case B is nearly symmetrical about the equator, the width of the eastward current band being about 3°. The bandwidth in case A is smaller, about 2°, and the symmetry appears somewhat distorted at this longitude, with the maximum eastward flow at 1°N. (In this respect it should be noted that the current bands of case A (Figure 6a) slant southeastward across the equator; at ~23°W the main eastward core is located on the equator, and at 10°W it is located near 2°S. The reason for this asymmetry is, as of yet, unknown but may have to do with Kelvin-Rossby wave interaction involving the Guinea coast parallel to the equator.) In neither case does the meridional profile of $\bar{u}$ correspond to the profile of $\bar{S}$. As is shown by Figures 3b and 3c, the meridional structure of the salinity tongue is broader than the band of eastward flow and biased toward the southern hemisphere. Apparently, this makes it difficult to reconcile the salinity pattern as a prime effect of mean advection and suggests a strong influence of diffusion.

At the present stage of modeling, prior to an understanding of model sensitivities to different parameter choices, we felt it to be premature for us to calculate complete, regional salinity budgets. However, some insight into the influence of different processes can be gained by simple scaling arguments. The essential question there seems to be the role the weak mean advection along the equator can play in the eastward extension of the equatorial salinity tongue.

Diffusive mechanisms of potential importance for the model pattern include the effect of subgrid turbulence as parametrized in the model by lateral and vertical eddy diffusivity, and the effect of velocity fluctuations resolved by the model. Since there is a strong difference between the mean salinity patterns of the coarse- and high-resolution models which use the same parameters for vertical diffusion, attention will be directed first to lateral mixing processes. We may get an estimate for the importance of the different friction schemes, if we consider their influence on a zonal salinity tongue of, say 200-km meridional scale. The biharmonic diffusion with $A_H^b = -2.5 \times 10^{19}$ cm^4 s^{-1} as used in cases A and B corresponds to a time scale for lateral mixing of $T_L^b \sim L_y^4/(-A_H^b) \sim 6 \times 10^4$ days. A Laplacian eddy diffusivity of $A_H = 0.5 \times 10^7$ cm^2 s^{-1} as used in case C below 2000 m has a much stronger impact: the respective frictional time scale can be estimated as $T_L \sim L_y^2/A_H \sim 115$ days. If that diffusivity should be balanced by a mean zonal advection, i.e., $\bar{u}(\partial\bar{S}/\partial x) \sim A_H(\partial^2\bar{S}/\partial y^2)$, we would need (if 1000 km is taken for the longitudinal scale of the salinity tongue) a mean flow $\bar{u}$ of $O(5$ cm s$^{-1})$. A lateral diffusivity of this magnitude obviously prohibits the evolution, or maintenance of an initially given salinity tongue. In contrast, an

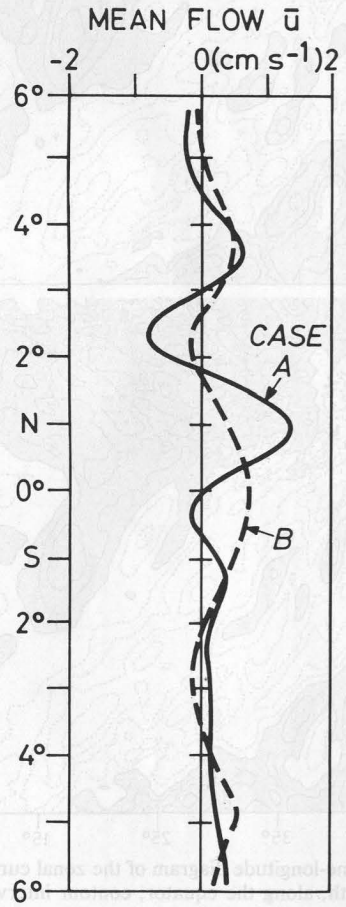

Fig. 10. Meridional profiles of the mean zonal velocity $\bar{u}$ along 30°W, 1875-m depth (cases A and B).

advective-diffusive balance in the biharmonic mixing case, i.e., $\bar{u}(\partial\bar{S}/\partial x) \sim -A_H^b(\partial^4\bar{S}/\partial y^4)$, would require a mean flow of only $O(10^{-2}$ cm s$^{-1})$. This order of magnitude consideration suggests that the explicit, lateral eddy diffusivity of the high-resolution model can probably be excluded as a process of leading order for the phenomena considered here.

A similar consideration applies for the vertical diffusivity. If we consider a vertical scale of ~500 m, the vertical mixing provided by the eddy coefficient $K_v = 0.3$ cm^2 s^{-1} as used in all three model cases would balance a zonal advection given by a mean flow of $O(10^{-2}$ cm s$^{-1})$. As the preceding model description has shown, the mean flow in the narrow band along the equator is 1 or 2 orders of magnitude higher. Accordingly, there must be other processes in the model which balance the mean zonal advection in the equatorial salinity tongue.

Potential important diffusive mechanism are provided by the deep velocity oscillations. Both components of the turbulent flux of salinity, i.e., $\overline{u'S'}$ and $\overline{v'S'}$, have a magnitude of $O(10^{-3})$ psu cm s^{-1} in the equatorial band and vary on scales of a few hundred kilometers, both along and across the equator. This implies flux divergences which locally exceed the model eddy diffusivity and, accordingly, must represent important contributors to the mean salinity budget. As an example, meridional profiles of $\overline{v'^2}$, and $\overline{v'S'}$ at 30°W are shown in Figure 11. The meridional velocity variance has a peak at the equator and a nearly symmetrical shape. The meridional flux reveals a divergent pattern at the equator, varying from -0.5×10^{-3} south, to 0.5×10^{-3} psu cm s^{-1} north of the equator, on a scale of about 2°. A spectral decomposition indicates that the 45-day waves do provide the main contribution to the velocity variance, but not to the turbulent flux $\overline{v'S'}$.

The meridional flux divergence of 0.5×10^{-10} psu s^{-1} could play a role in the mean salinity budget near the equator. If we assume a balance for the salt tongue between mean zonal advection and meridional diffusion of the form $\bar{u}\,\partial\bar{S}/\partial x \sim \partial/\partial y\ \overline{v'S'}$, and take an estimate (from Fig. 3) for $\partial\bar{S}/\partial x$ of 2×10^{-10} psu cm^{-1}, we get $\bar{u}$ of 0.25 cm s^{-1}. This estimate is similar to the actual mean zonal velocity in the equatorial band of model cases A and B. It has to be noted, however, that the turbulent flux components vary both across and along the equator. Actual budgets might well be more complicated and involve more than two terms. This fact is amplified by the asymmetric shape of the salinity tongue with respect to the equator despite the concentration of eastward advection near the equator. The simple order of magnitude considerations nevertheless suggest that the weak zonal flow does play a leading role for the salinity pattern near the equator.

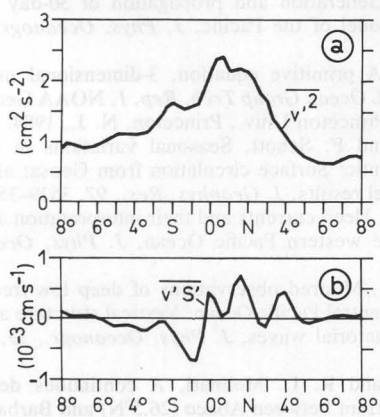

Fig. 11. Meridional profiles along 30°W, 1875-m depth (case A): (*a*) meridional velocity variance $\overline{v'^2}$ and (b) turbulent flux of salinity $v'S'$.

5. Summary and Conclusion

Deep equatorial current oscillations in the high-resolution model are essentially of two types: The first is an oscillation predominantly of meridional velocity of about 1000-km wavelength, with westward phase and eastward group velocity, indicative of Rossby-gravity waves. Their existence has been attributed to instabilities of the upper current system [e.g., *Cox*, 1980; *Philander et al.*, 1986]. Their longer period compared with the previous multilevel model studies (45 days instead of 30 days) indicates differences in the stability properties of the upper layer flow system. Their generation and properties need further investigation.

The second type is a deep response to the seasonal variation of the wind forcing in the equatorial Atlantic, with kinetic energy mainly in the zonal component, a basin-wide zonal scale, and westward phase propagation of about 15 cm s^{-1}. While the mechanism of the deep zonal current generation seems to be present both in the high- and coarse-resolution cases (A and C), amplitudes are very weak (<0.5 cm s^{-1}) in the latter one. A strong influence of the larger horizontal friction of case C can be expected due to the small meridional scale of the current bands, being near the resolution limit of the 1° grid.

The main problem when assessing the relevance of the high-resolution model results is the sparsity of deep current data from the equatorial Atlantic as regards both spatial structure and time scales. Measurements using continuous profiling instruments have provided evidence of complex zonal current structures beneath the equatorial undercurrents. Deep zonal jets were first discovered in the Indian [*Luyten and Swallow*, 1976] and Pacific oceans [*Eriksen*, 1981]; in contrast to the present model results, they are characterized by short vertical scales, of a few hundred meters, and long time scales, up to several years [*Firing*, 1987; *Ponte and Luyten*, 1989, 1990]. Velocity profiles in the deep equatorial Atlantic have been obtained only very recently. The measurements at 30°W (Figure 2*a*) indicated predominantly zonal currents, alternating in east-west direction with depth, but of larger vertical scale than in the Pacific and Indian oceans [*Ponte et al.*, 1990]. The present model does not capture the essential features of a stacked jet system, notably its complex vertical mode structure; obviously it cannot contribute to resolving the issue of the origin of these jets.

Concerning an annual signal in the deep equatorial Atlantic as shown by the model, there is at present no solid evidence. Of the two profiles from the equatorial Atlantic at 30°W (Figure 2*a*) it can only be stated that they do not rule out the possibility of an annual oscillation there; further east, the deep current meter record (Figure 2*b*) does not indicate a significant contribution of an annual cycle. Yearlong deep moored current measurements have been obtained recently at various levels at 44°W along the western boundary in the equatorial Atlantic [*Schott et al.*, 1993]. While a significant

annual signal was not detected, the presence of an annual signal of a few centimeters per second cm s^{-1} amplitude hidden in the strong mesoscale variability of 10–20 cm $^{-1}$ rms amplitude could not be excluded. Near the western boundary the model velocities are also dominated by higher-frequency fluctuations (Figure 7); however, these are highly repetitive from year to year and apparently in close phase relation with the mean seasonal forcing.

In the deep western Indian Ocean, where strong annual monsoonal forcing acts at the surface, the evidence for an annual cycle was ambivalent: while the annual cycle in the boundary current was small at 1000 m and indistinguishable from zero at 2000 m, a significant seasonal reversal was found in one record at 3000-m depth [*Schott et al.*, 1989]. On the other hand, indications for a wind-induced seasonal signal have been found in the deep equatorial Pacific. Two-year time series from deep-sea moorings in the central equatorial Pacific showed that variability at annual and shorter periods existed that was of larger vertical scales than the deep jets [*Eriksen*, 1985]. Observations of the subthermocline thermal structure in the central Pacific Ocean showed a vertically propagating signal of annual period that was attributed to a wind-forced Rossby wave [*Lukas and Firing*, 1985]. Additional evidence of such waves has recently been inferred from an analysis of historical hydrographic data in the Pacific [*Kessler*, 1991]; the upward phase propagation suggested a surface source for the annual waves.

A remarkable feature of the high-resolution model is the tongue of saline NADW extending eastward along the equator. This model pattern does resemble the distribution of deepwater properties such as oxygen [*Wüst*, 1935], nitrate and silicate [*Kawase and Sarmiento*, 1986], or chlorofluoromethane [*Weiss et al.*, 1985] in the equatorial Atlantic. The observed patterns suggested that some NADW carried southward by the DWBC separates from the western boundary and spreads eastward. At this point it is interesting to note that the eastward salinity wedge in the model does occur without being associated with a clear bifurcation of the western boundary current: the model flow field is dominated by a DWBC with core velocities exceeding 10 cm s^{-1}, crossing the equator with almost no interruption, while only a very weak mean flow, with a maximum velocity of 1 cm s^{-1}, extends eastward along the equator. This current is present in both high-resolution experiments. The strong annual oscillations in case A seem to somewhat distort the symmetry of the mean eastward current but do not appear to be essential for its existence.

This weak zonal flow appears consistent with the vestigial eastward current obtained by *Kawase et al.* [1992] in a numerical experiment on the encounter of a DWBC with the equator. Extending the earlier study of *Kawase* [1987] of the spin-up of abyssal ocean circulation, their model results emphasized that there can be no significant bifurcation of a steady state western boundary flow at the equator. During the spin-up of deep circulation an eastward current develops in the wake of Kelvin waves traveling along the equator; subsequently, however, the equatorial boundary layer broadens and eventually disappears as a result of long Rossby waves traveling back from the eastern boundary. In this scenario, unless unrealistically strong wave damping is considered, an eastward flow can be achieved only as a transient in the initial adjustment phase of the deep circulation. After 10 years of spin-up in the *Kawase et al.* [1992] experiment, there remained an eastward current at the equator of only 3 cm s^{-1}. It needs to be investigated in further, extended model integrations whether the mean equatorial current in the CME experiments represents a remnant of the spin-up (20 years) according to the scenario of Kawase, or whether other dynamical factors contribute to its existence.

The main conclusion to be drawn here is that even a weak mean flow of O(1 cm s^{-1}) may have a significant effect on tracer distributions along the equator. The scale analysis of the model results indicates that the mean eastward currents of the high-resolution cases A and B seem sufficient to set up an advective-diffusive balance in this region. Instead, in the low-resolution model case the balance was shown to be essentially diffusive, implying that the presence also in that model of a weak eastward mean current (~0.25 cm s^{-1}) could not cause a salinity tongue along the equator. It seems likely that quantitative details of the salinity budget and, accordingly, the shape of the salinity tongue are sensitive to model parameters such as frictional coefficients, grid sizes, etc., which will affect the intensity of the turbulent fluctuations. Before starting efforts to calculate a complete salinity budget of a given numerical model solution, it would appear important to further examine these model dependencies.

Acknowledgments. We thank Joseph L. Reid for permission to use some of his unpublished work on property distributions in the deep Atlantic Ocean. We are grateful to F. Bryan and W. Holland for providing the model code and sharing their experience from the initial experiments of the U.S. WOCE Community Modeling Effort. Thanks are also due to R. Döscher, R. Budich, P. Herrmann, and M. Hamann for help in running and analyzing the numerical models on the Cray X-MP of Kiel University.

REFERENCES

Böning, C. W., R. Döscher and R. G. Budich, Seasonal transport variation in the western subtropical North Atlantic: Experiments with an eddy-resolving model, *J. Phys. Oceanogr.*, *21*, 1271–1289, 1991.

Bryan, F. O., and W. R. Holland, A high-resolution simulation of the wind- and thermohaline driven circulation in the North Atlantic Ocean, in *Parameterization of Small-Scale Processes, Proceedings 'Aha Huliko'a Hawaiian Winter Workshop*, edited by P. Müller and D. Henderson, pp. 99–115, University of Hawaii, Honolulu, 1989.

Bryan, K., A numerical method for the study of the circulation of the world ocean, *J. Comput. Phys.*, *4*, 347–376, 1969.

Cox, M. D., Generation and propagation of 30-day waves in a numerical model of the Pacific, *J. Phys. Oceanogr.*, *10*, 1168–1186, 1980.

Cox, M. D., A primitive equation, 3-dimensional model of the ocean, *GFDL Ocean Group Tech. Rep. 1*, NOAA Geophys. Fluid Dyn. Lab., Princeton Univ., Princeton, N. J., 1984.

Didden, N., and F. Schott, Seasonal variations in the western tropical Atlantic: Surface circulation from Geosat altimetry and WOCE model results, *J. Geophys. Res.*, *97*, 3529–3542, 1992.

Eriksen, C. C., Deep currents and their interpretation as equatorial waves in the western Pacific Ocean, *J. Phys. Oceanogr.*, *11*, 48–70, 1981.

Eriksen, C. C., Moored observations of deep low-frequency motions in the central Pacific Ocean: Vertical structure and interpretation as equatorial waves, *J. Phys. Oceanogr.*, *15*, 1085–1113, 1985.

Fine, R. A., and R. L. Molinari, A continuous deep western boundary current between Abaco (26.5°N) and Barbados (13°N), *Deep Sea Res.*, *35*, 1441–1450, 1988.

Firing, E., Deep zonal currents in the central equatorial Pacific, *J. Mar. Res.*, *45*, 791–812, 1987.

Han, Y., A numerical world ocean general circulation model, II, *Dyn. Atmos. Oceans*, *8*, 141–172, 1984.

Hellerman, S., and M. Rosenstein, Normal monthly wind stress over the world ocean with error estimates, *J. Phys. Oceanogr.*, *13*, 1093–1104, 1983.

Kawase, M., Establishment of deep ocean circulation driven by deep-water production, *J. Phys. Oceanogr.*, *17*, 2294–2317, 1987.

Kawase, M., and J. L. Sarmiento, Circulation and nutrients in middepth Atlantic waters, *J. Geophys. Res.*, *91*, 9749–9770, 1986.

Kawase, M., L. M. Rothstein, and S. R. Springer, Encounter of a deep western boundary current with the equator: A numerical spin-up experiment, *J. Geophys. Res.*, *97*, 5447–5463, 1992.

Kessler, W. S., Vertical-propagating annual Rossby waves observed below the thermocline in the equatorial Pacific, paper presented at XX General Assembly, Int. Union of Geod. and Geophys., Vienna, 1991.

Levitus, S., Climatological atlas of the world ocean, *NOAA Tech. Pap. 13*, 173 pp., U.S. Govt. Print. Off., Washington, D. C., 1982.

Lukas, R., and E. Firing, The annual Rossby wave in the central equatorial Pacific, *J. Phys. Oceanogr.*, *15*, 55–67, 1985.

Luyten, J. R., and J. C. Swallow, Equatorial undercurrents, *Deep Sea Res.*, *23*, 1005–1007, 1976.

McCreary, J. P., and Z. Yu, Equatorial dynamics in a $2\frac{1}{2}$ layer model. *Prog. Oceanogr.*, *29*, 61–132, 1992.

Philander, S. G. H., W. J. Hurlin, and R. C. Pacanowski, Properties of long equatorial waves in models of the seasonal cycle in the tropical Atlantic and Pacific oceans, *J. Geophys. Res.*, *91*, 14,207–14,211, 1986.

Ponte, R. M., and J. Luyten, Analysis and interpretation of deep equatorial currents in the central Pacific, *J. Phys. Oceanogr.*, *19*, 1025–1038, 1989.

Ponte, R. M., and J. Luyten, Deep velocity measurements in the western equatorial Indian Ocean, *J. Phys. Oceanogr.*, *20*, 44–52, 1990.

Ponte, R. M., J. Luyten, and P. L. Richardson, Equatorial deep jets in the Atlantic Ocean, *Deep Sea Res.*, *37*, 711–713, 1990.

Richardson, P. L., and W. J. Schmitz, Jr., Deep cross-equatorial flow in the Atlantic measured with SOFAR floats, *J. Geophys. Res.*, in press, 1993

Semtner, A. J., and R. M. Chervin, Ocean general circulation from a global eddy-resolving model, *J. Geophys. Res.*, *97*, 5493–5550, 1992.

Schott, F., and C. W. Böning, The WOCE model in the western equatorial Atlantic: Upper layer circulation, *J. Geophys. Res.*, *96*, 6993–7004, 1991.

Schott, F., J. Swallow, and M. Fieux, Deep currents underneath the equatorial Somali Currents, *Deep Sea Res.*, *36*, 1191–1199, 1989.

Schott, F., J. Fischer, J. Reppin, and U. Send, On mean and seasonal currents and transports at the western boundary of the equatorial Atlantic, *J. Geophys. Res.*, in press, 1993.

Weisberg, R. H., and A. M. Horigan, Low frequency variability in the equatorial Atlantic, *J. Phys. Oceanogr.*, *11*, 913–920, 1981.

Weiss, R. F., J. L. Bullister, R. H. Gammon, and M. J. Warner, Atmospheric chlorofluoromethanes in the deep equatorial Atlantic, *Nature*, *314*, 608–610, 1985.

Wüst, G., Schichtung und Zirkulation des Atlantischen Ozeans: Die Stratosphäre, *Wiss. Ergeb. Dtsch. Atlant. Exp. Meteor 1925–1927*, *6*, 180 pp., 1935.

C. W. Böning and F. A. Schott, Institut für Meereskunde an der Universität Kiel, Düsternbrooker Weg 20, D-2300 Kiel 1, Germany.

(Received March 13, 1992;
revised July 17, 1992;
accepted October 28, 1992.)